Symmetric alignment of the nematic matrix between close penetrable colloidal particles

2004 J. Phys.: Condens. Matter 16 S1969

(http://iopscience.iop.org/0953-8984/16/19/009)

INSTITUTE OF PHYSICS PUBLISHING JOURNAL OF PHYSICS: CONDENSED MATTER

J. Phys.: Condens. Matter **16** (2004) S1969–S1980 PII: S0953-8984(04)75613-1

Symmetric alignment of the nematic matrix between close penetrable colloidal particles

P I C Teixeira[1], **F Barmes**[2] **and D J Cleaver**[3]

[1] Faculdade de Engenharia, Universidade Católica Portuguesa, Estrada de Talaíde, P-2635-631 Rio de Mouro, Portugal
[2] Centre Européen de Calcul Atomique et Moléculaire (CECAM), ENS-Lyon, 46, allée d'Italie, 69007 Lyon, France
[3] Materials Research Institute, Sheffield Hallam University, Pond Street, Sheffield S1 1WB, UK

Received 28 January 2004
Published 30 April 2004
Online at stacks.iop.org/JPhysCM/16/S1969
DOI: 10.1088/0953-8984/16/19/009

Abstract

A simple model is proposed for the liquid crystal matrix surrounding 'soft' colloidal particles whose separation is much smaller than their radii. We use our implementation of the Onsager approximation of density-functional theory (Chrzanowska *et al* 2001 *J. Phys.: Condens. Matter* **13** 4715) to calculate the structure of a nanometrically thin film of hard Gaussian overlap particles of elongations $\kappa = 3$ and 5, confined between two solid walls. The penetrability of either substrate can be tuned independently to yield symmetric or hybrid alignment. Comparison with Monte Carlo simulations of the same system (Cleaver and Teixeira 2001 *Chem. Phys. Lett.* **338** 1, Barmes and Cleaver 2004 in preparation) reveals good agreement in the symmetric case.

1. Introduction

A *nematic colloid*, sometimes called an *inverted nematic emulsion*, is a dispersion of isotropic particles, either rigid (grains) or deformable (e.g., water droplets), in a nematic liquid crystal (LC) [1]. Because the nematic director is anchored on the surface of the (nearly always quasi-spherical) inclusions, distortions of the director field are induced which in turn give rise to effective interactions between the inclusions themselves. These can be manipulated by treating the walls of the container, applying fields, or coating the surfaces of the colloidal particles, in order to produce various states of aggregation, e.g., strings along the director lines [2]. Nematic colloids are therefore ideal model systems to study topological defects, and one important practical application appears to be the suspension of abrasive particles in lyotropic mesophases. In a newer variant, inclusions of size exceeding the cholesteric pitch (radius $\sim$1 μm) are dispersed in a well-aligned cholesteric sample. Here the colloidal particles stabilize a network of defects by residing at its nodes, thereby transforming the cholesteric liquid into a new type of material exhibiting gel-like rheological properties [3]. This study was later extended to the simpler system consisting of smaller (radii 150–200 nm) particles in

a nematic host: upon quenching the initial homogeneously-mixed colloid from the isotropic (I) to the nematic (N) state, the particles were seen to phase-separate and aggregate into thin walls, bounding domains of practically pure nematic LC [4]. The resulting metastable, but relatively long-lived, cellular structure exhibited dramatically enhanced mechanical strength, with an elastic modulus $G' \geqslant 10^5$ Pa and a well-defined yield stress, which are functions of particle concentration.

In all the above, the colloidal particles are much larger than the LC molecules, which can then be regarded as a continuum background. Effective interaction potentials between colloidal particles have been derived, analytically in some limits, more generally numerically, using either Frank theory (below the I–N transition) [2, 5] or Landau–de Gennes (LdG) theory (above the I–N transition) [6]; more recent work considered van der Waals, steric, electrostatic and LC-mediated contributions [7]. However, continuum-based approaches are expected to fail when the interparticle separation becomes of the order of a few LC molecular sizes, as in fully-formed aggregates. Furthermore, especially in the case of LdG theory, the solution method is heavy, and affords little insight into the physics of the problem. Finally, evaluation of the three- and more-particle contributions (these effective potentials being in general not pairwise additive) becomes prohibitively complicated [6]: one would like to be able to obtain the different terms as functions of the microscopic potential parameters, and in a systematic, well-controlled manner.

The complexity of the task in hand requires that we start our attack from the very beginning: take the simplest molecular model of a LC and squeeze it to nanometric thickness; then find the free energy dependence on particle separation, and hence the effective interaction. Here we carry out only the first part of this programme, leaving the second for future work. In a previous paper [8] we showed how the simple Onsager approximation of density-functional theory could provide a semi-quantitatively accurate description of the structure of a fluid of hard rods confined between two hard, impenetrable walls, provided allowance was made, in a phenomenological way, for the incorrect prediction of the location of the isotropic–nematic (I–N) transition. In the present paper we apply the same strategy to symmetric films confined between flat substrates of variable penetrability, in order to mimic different anchoring conditions. This is not unreasonable as a first approach, in view of the large disparity of the typical length scales of LC molecules—a few nanometres—and inclusions—hundreds of nanometres (but see [9] for an attempt to consider curved hard surfaces).

This paper is organized as follows. In section 2 we recapitulate the theory of [8] and extend it to the case of unequal anchorings at the confining walls. Then in section 3 we present results for the density and order parameter profiles of LC films subject to symmetrical anchoring conditions, and compare them with those obtained by Monte Carlo (MC) simulation [10, 11]. Finally, in section 4 we discuss the potential and limitations of our approach, and outline some directions for future research.

2. Theory

As before, we take as a representation of uniaxial rod-like particles the hard Gaussian overlap (HGO) potential used previously in 3d bulk simulations and Onsager theory of lyotropic LC behaviour [12, 13] (i.e., where the LC phase transitions are driven by density, rather than temperature, changes):

$$U_{12}(\mathbf{r}_{12}, \omega_1, \omega_2) = \begin{cases} 0 & \text{if } r_{12} \geqslant \sigma(\hat{\mathbf{r}}_{12}, \omega_1, \omega_2) \\ \infty & \text{if } r_{12} < \sigma(\hat{\mathbf{r}}_{12}, \omega_1, \omega_2), \end{cases} \tag{1}$$

where $\omega_i = (\theta_i, \phi_i)$ are the polar and azimuthal angles describing the orientation of the long axis of particle i, and $\hat{\mathbf{r}}_{12} = \mathbf{r}_{12}/r_{12}$ is a unit vector along the line connecting the centres of the two particles. The range parameter function is given by

$$\sigma(\hat{\mathbf{r}}_{12}, \omega_1, \omega_2) = \sigma_0 \left[1 - \frac{1}{2}\chi \left\{ \frac{(\hat{\mathbf{r}}_{12} \cdot \hat{u}_1 + \hat{\mathbf{r}}_{12} \cdot \hat{u}_2)^2}{1 + \chi(\hat{u}_1 \cdot \hat{u}_2)} + \frac{(\hat{\mathbf{r}}_{12} \cdot \hat{u}_1 - \hat{\mathbf{r}}_{12} \cdot \hat{u}_2)^2}{1 - \chi(\hat{u}_1 \cdot \hat{u}_2)} \right\} \right]^{-1/2}, \tag{2}$$

where $\hat{u}_i = (\cos\phi_i \sin\theta_i, \sin\phi_i \sin\theta_i, \cos\theta_i)$ and $\chi = (\kappa^2 - 1)/(\kappa^2 + 1)$, κ being the particle length to breadth ratio, σ_L/σ_0. For moderate κ, the HGO model is a good approximation to the hard ellipsoid (HE) contact function [14, 15]; furthermore, their virial coefficients (and thus their equations of state, at least at low to moderate densities) are very similar [16]. However, this is no longer true of highly non-spherical particles [17], for which the behaviour of the two models differs appreciably [13]: here we restrict ourselves to $\kappa = 3$ and 5. Finally, HGOs have the considerable computational advantage over HEs that $\sigma(\hat{\mathbf{r}}_{12}, \omega_1, \omega_2)$, the distance of closest approach between two particles, is given in closed form.

Particle–substrate interactions have been modelled, as in [10, 11], by a hard needle–wall potential:

$$U_{\text{wall}}(z, \theta) = \begin{cases} 0 & \text{if } |z - z_0| \geqslant \frac{L}{2}\cos\theta \\ \infty & \text{if } |z - z_0| < \frac{L}{2}\cos\theta, \end{cases} \tag{3}$$

where the z-axis has been chosen to be perpendicular to the substrate, located at z_0, and $0 \leqslant L \leqslant \sigma_L$ sets the length of the needle with which the substrate interacts. Here, L affords us a degree of control over the anchoring properties: physically, $0 < L < \sigma_L$ corresponds to a system where the molecules are able to embed their side groups, but not the whole length of their cores, into the bounding walls. Varying L between 0 and σ_L is therefore equivalent to changing the degree of penetrability of the substrates in an experimental situation, e.g., by manipulating the density or the orientation of an adsorbed surface layer. This can be done independently at either substrate, whereby symmetric or hybrid anchoring conditions can be obtained.

The equilibrium density distribution of an HGO film is that which minimizes its grand-canonical functional [18]:

$$\begin{aligned} \beta\Omega[\rho(\mathbf{r}, \omega)] &= \beta\mathcal{F}[\rho(\mathbf{r}, \omega)] + \beta \int \left[\sum_{\alpha=1}^{2} U_{\text{wall}}(\theta, |z - z_0^\alpha|) - \mu \right] \rho(\mathbf{r}, \omega)\, \mathrm{d}\mathbf{r}\, \mathrm{d}\omega \\ &= \int \rho(\mathbf{r}, \omega)[\log \rho(\mathbf{r}, \omega) - 1]\, \mathrm{d}\mathbf{r}\, \mathrm{d}\omega \\ &\quad - \tfrac{1}{2} \int \rho(\mathbf{r}_1, \omega_1) f_{12}(\mathbf{r}_1, \omega_1, \mathbf{r}_2, \omega_2) \rho(\mathbf{r}_2, \omega_2)\, \mathrm{d}\mathbf{r}_1\, \mathrm{d}\omega_1\, \mathrm{d}\mathbf{r}_2\, \mathrm{d}\omega_2 \\ &\quad + \beta \int \left[\sum_{\alpha=1}^{2} U_{\text{wall}}(|z - z_0^\alpha|, \theta) - \mu \right] \rho(\mathbf{r}, \omega)\, \mathrm{d}\mathbf{r}\, \mathrm{d}\omega, \end{aligned} \tag{4}$$

where $\mathcal{F}[\rho(\mathbf{r}, \omega)]$ is the intrinsic Helmholtz free energy of the inhomogeneous fluid, $f_{12}(\mathbf{r}_1, \omega_1, \mathbf{r}_2, \omega_2) = \exp[-\beta U_{12}(\mathbf{r}_1, \omega_1, \mathbf{r}_2, \omega_2)] - 1$ is its Mayer function, μ is the chemical potential, z_0^α ($\alpha = 1, 2$) are the positions of the two substrates, and, because we are dealing with hard-body interactions only, for which the temperature is an irrelevant variable, we can set $\beta = 1/k_{\text{B}}T = 1$ in all practical calculations (we retain it in the formulae for generality). $\rho(\mathbf{r}, \omega)$ is the density-orientation profile in the presence of the external potential $U_{\text{wall}}(z, \theta)$; it is normalized to the total number of particles N,

$$\int \rho(\mathbf{r}, \omega)\, \mathrm{d}\mathbf{r}\, \mathrm{d}\omega = N, \tag{5}$$

and is related to the probability that a particle positioned at $\mathbf{r}$ has orientation between ω and $\omega+\mathrm{d}\omega$. From equation (1) it follows that the interaction term in equation (4) is just the excluded volume of two HGO particles, weighted by the density-orientation distributions $\rho(\mathbf{r}, \omega)$. This equation constitutes the Onsager approximation to the free energy of the confined HGO fluid.

Because the particle–substrate interaction, equation (3), only depends on z and θ, it is reasonable to assume that there is no in-plane structure, so that all quantities are functions of z only. Then equation (4) simplifies to

$$\begin{aligned}\frac{\beta\Omega\left[\rho(z,\omega)\right]}{S_{xy}} &= \int \rho(z,\omega)\left[\log\rho(z,\omega)-1\right]\mathrm{d}z\,\mathrm{d}\omega \\ &\quad -\tfrac{1}{2}\int \rho(z_1,\omega_1)\Xi(z_1,\omega_1,z_2,\omega_2)\rho(z_2,\omega_2)\,\mathrm{d}z_1\,\mathrm{d}\omega_1\,\mathrm{d}z_2\,\mathrm{d}\omega_2 \\ &\quad +\beta\int\left[\sum_{\alpha=1}^{2}U_{\mathrm{wall}}(|z-z_0^{\alpha}|,\theta)-\mu\right]\rho(z,\omega)\,\mathrm{d}z\,\mathrm{d}\omega, \end{aligned} \tag{6}$$

where S_{xy} is the interfacial area. $\Xi(z_1, \omega_1, z_2, \omega_2)$ is now the area of a slice (cut parallel to the bounding plates) of the excluded volume of two HGO particles of orientations ω_1 and ω_2 and centres at z_1 and z_2 [19], for which an analytical expression has been derived [20]. Note that each surface particle experiences an environment that has both polar *and* azimuthal anisotropy, as a consequence of the excluded-volume interactions between the particles in addition to the 'bare' wall potential.

Minimization of the grand canonical functional, equation (6),

$$\frac{\delta\Omega\left[\rho(z,\omega)\right]}{\delta\rho(z,\omega)}=0, \tag{7}$$

yields the Euler–Lagrange equation for the density-orientation profile,

$$\log\rho(z,\omega)=\beta\mu-\int'\Xi(z,\omega,z',\omega')\rho(z',\omega')\,\mathrm{d}z'\,\mathrm{d}\omega', \tag{8}$$

where the effect of the wall potentials, given by equation (3), has been incorporated through restriction of the range of integration over θ:

$$\int'\mathrm{d}\omega=\int_0^{2\pi}\mathrm{d}\phi\int_{\pi-\theta_m}^{\theta_m}\sin\theta\,\mathrm{d}\theta=\int_0^{2\pi}\mathrm{d}\phi\int_{-\cos\theta_m}^{\cos\theta_m}\mathrm{d}x, \tag{9}$$

with

$$\cos\theta_m=\begin{cases}1 & \text{if } |z-z_0|\geqslant\frac{L}{2}\\ \dfrac{|z-z_0|}{L/2} & \text{if } |z-z_0|<\frac{L}{2},\end{cases} \tag{10}$$

z_0 being, we recall, the position of a substrate.

It is clear from the structure of equation (8) that μ is the Lagrange multiplier associated with requiring that the mean number of particles in the system be N. We are therefore at liberty to fix either μ or N (see also the discussion in [22]): as in earlier work we opt for the latter, since it allows closer contact with (constant NVT) simulation.

Once $\rho(\omega, z)$ has been found, we can integrate out the angular dependence to get the density profile,

$$\rho(z)=\int\rho(z,\omega)\,\mathrm{d}\omega, \tag{11}$$

Table 1. Bulk I–N coexistence densities of HGOs from theory (th) [8] and simulation (sim) [13].

κ	$\rho_{\mathrm{I}}^{*,\mathrm{th}}$	$\rho_{\mathrm{N}}^{*,\mathrm{th}}$	$\rho_{\mathrm{I}}^{*,\mathrm{sim}}$	$\rho_{\mathrm{N}}^{*,\mathrm{sim}}$
3	0.830 100	0.864 356	0.2990	0.3046
5	0.210 731	0.234 746	0.1192	0.1275

and use this result to define the orientational distribution function (ODF) $\hat{f}(z,\omega) = \rho(z,\omega)/\rho(z)$, from which we can calculate the orientational order parameters in the laboratory-fixed frame [23]:

$$\eta(z) = \langle P_2(\cos\theta)\rangle = Q_{zz}, \tag{12}$$

$$\varepsilon(z) = \langle \sin 2\theta\ \sin\phi\rangle = \tfrac{4}{3}Q_{yz}, \tag{13}$$

$$\nu(z) = \langle \sin 2\theta\ \cos\phi\rangle = \tfrac{4}{3}Q_{xz}, \tag{14}$$

$$\varsigma(z) = \langle \sin^2\theta\ \cos 2\phi\rangle = \tfrac{2}{3}(Q_{xx} - Q_{yy}), \tag{15}$$

$$\tau(z) = \langle \sin^2\theta\ \sin 2\phi\rangle = \tfrac{4}{3}Q_{xy}, \tag{16}$$

where $\langle\mathcal{A}\rangle = \int \mathcal{A}\hat{f}(z,\omega)\,\mathrm{d}\omega$. These are the five independent components of the nematic order parameter tensor, $Q_{\alpha\beta} = \langle\frac{1}{2}(3\hat{\omega}_\alpha\hat{\omega}_\beta - \delta_{\alpha\beta})\rangle$: they give the fraction of molecules oriented along the z-axis (Q_{zz}); along the bisectors of the yz-, xz- and xy-quadrants (Q_{yz}, Q_{xz} and Q_{xy}, respectively); and the difference between the fractions of molecules oriented along the x- and y-axes ($Q_{xx} - Q_{yy}$). In the case under study there is no twist, i.e., the director is confined to a plane that we can take as the xz plane and $\varepsilon(z) = \tau(z) = 0$. The three remaining order parameters, $\eta(z)$, $\nu(z)$ and $\varsigma(z)$, are in general all non-zero owing to surface-induced biaxiality; see our earlier work for $L = \sigma_L$ [8]. This effect has not been neglected in the present treatment, but in what follows we show results for $\eta(z) = Q_{zz}$ only, as we wish to concentrate on the planar-to-homeotropic transition.

3. Results

In earlier work [8] we found that the second-virial approximation does not give an accurate prediction for the location or the width of the I–N transition of particles of moderate elongation, as the contribution of higher virial coefficients is then substantial. Therefore it does not make much sense to perform comparisons of theory and simulation at the same density. To circumvent this difficulty we have, as in a previous paper, resorted to extending a phenomenological scaling originally proposed by McDonald *et al* [24] in the context of the I–N interface: comparison is instead effected between state points from theory and simulation characterized by the same $d_{\mathrm{bulk}} \equiv (\rho_{\mathrm{bulk}} - \rho_{\mathrm{I}})/(\rho_{\mathrm{N}} - \rho_{\mathrm{I}})$. Table 1 lists the I–N coexistence densities we have used, obtained from the theory of [8], and from thermodynamic integration of a 500-particle system [13]. The latter results are in reasonably good agreement with those of two MC studies: the earlier constant-NpT simulation of a 256-particle system by Padilla and Velasco [12], and the later constant-NVT/NpT simulations of a 1000-particle system by two of us [11].

We emphasize that there is no fundamental reason why such a scaling should work, and that a proper validation would require both a more sophisticated theoretical treatment (along the lines of, e.g., [25] or [26]) and a more reliable location by MC of the I–N transition of the confined HGO fluid, to allow for a possible shift relative to the bulk ('capillary nematization') [11, 27, 28]. Still, we regard the procedure adopted as the best working tool for comparison of these systems that is available at the moment. The unscaled densities at which simulation runs and theory calculations have been performed are collected in table 2.

Table 2. Scaled densities d_{bulk} used in figures 1–4 for comparison of theory (th) and simulation (sim) results: d_{bulk} is positive (negative) in the bulk nematic (isotropic) phase. $\rho^{*,\text{th}}$ and $\rho^{*,\text{sim}}$ are the unscaled densities at which the theoretical calculations and the simulations have been performed.

κ	d_{bulk}	$\rho^{*,\text{th}}$	$\rho^{*,\text{sim}}$
3	−3.392 852 98	0.713 874 491	0.28
3	7.321 422 42	1.080 902 51	0.34
5	−1.108 433 72	0.184 111 97	0.11
5	2.506 024 58	0.270 913 166	0.14

Equation (8) was solved iteratively for $\rho(z, \omega)$ by the Picard method, with an admixture parameter of 0.9 (i.e., 90% of 'old' solution in each iteration), starting from a uniform and isotropic profile. Following Chrzanowska [21], integrations were performed by Gauss–Legendre quadrature, using 64 z-points (the minimum necessary to resolve the structure of profiles at the higher densities considered) and 16×16 ω-points (for consistence with the bulk calculation reported in [8]). Note that the range of ω' depends on z': the closer a particle is to a substrate, the fewer orientations are accessible. In order to achieve good accuracy it is nevertheless crucial to include the same number of points in the angular integrations for all z' [21]. Convergence was deemed to have been achieved when the error, defined as the sum of the absolute values of differences between consecutive iterates at $64 \times 16 \times 16 = 16\,384$ points, was less than 10^{-1}. The density and order parameter profiles were then calculated from equations (11) and (12)–(16), respectively. Details of the simulations have been published elsewhere [10, 11].

In figure 1 we plot $d(z)$ and $Q_{zz}(z)$ profiles for a symmetrical film of HGO particles of elongation $\kappa = 5$ and $L^* = L/\sigma_0 = 3.0$, which exhibits uniform planar alignment [10, 11]. Equilibrium density peak formation is captured reasonably well by theory, which however underestimates the height of the peaks and the depth of the troughs, especially at the higher density. For $d_{\text{bulk}} = -1.108\,433\,72$, $Q_{zz}(z)$ is everywhere zero except in the surface layers (the high-density peaks at $|z - z_0^\alpha| \sim 0$, $\alpha = 1, 2$), by which we mean the regions where the rotational freedom of a particle is restricted by the presence of the walls. Because the walls are impenetrable to a 'needle' of length L (see equation (3)), the thickness of these layers is $\sim L/2 = 1.5\sigma_0$: in order to reside there a particle has to be parallel to the wall; hence $Q_{zz}(z) < 0$. We speculate that the $Q_{zz}(z)$ peaks at $|z - z_0^\alpha| \sim L/2$ are due to excluded volume effects: particles are unable to minimize their free energy by retaining full rotational freedom, and thus give rise to a zero order parameter, by the presence of the adsorbed surface layers at $|z - z_0^\alpha| \leqslant L/2$. It is then advantageous for them to align homeotropically so as to stick their ends through the wall and thereby decrease the total excluded volume inside the system. At the higher density $d_{\text{bulk}} = 2.506\,024\,58$ there is again good agreement between theory and simulation for $Q_{zz}(z)$, presumably because the degree of order is now quite large and close to saturation.

Figure 2 shows the same quantities but for $L^* = 2.0$, for which alignment is perpendicular to the walls [10, 11]. The density peaks, the highest of which now occur at $|z - z_0^\alpha| \sim L/2 = \sigma_0$, are even more pronounced than for $L^* = 3.0$, and likewise underestimated by theory. In particular, simulation appears to show the formation of some five layers, whereas theory bears out only four. The $Q_{zz}(z)$ profiles from both theory and simulation are very similar to those for $L^* = 3.0$ at the lower density, but theory overestimates the degree of order at the higher density.

Figures 3 and 4 illustrate planar and homeotropic alignment for the smaller elongation $\kappa = 3$; now the Onsager approximation is expected to fare worse, and indeed it underestimates

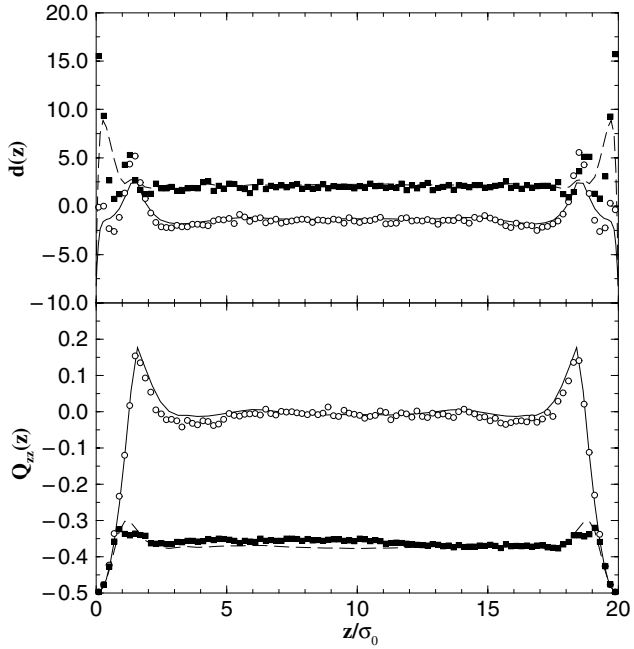

Figure 1. Scaled density $d(z)$ (top) and order parameter $Q_{zz}(z)$ (bottom) profiles for a symmetrical film of HGO particles of elongation $\kappa = 5$ and $L^* = 3.0$ ($L/\sigma_L = 0.6$), for $d_{\text{bulk}} = -1.108\,433\,72$ (solid curve and circles) and $2.506\,024\,58$ (dashed curve and squares). Lines are from theory, symbols are from simulation. At the higher density, which lies in the nematic region of the bulk phase diagram, alignment is planar throughout the film, as shown by the fact that $Q_{zz}(z) < 0$ everywhere. See the text and table 2 for details.

the structure of the density profiles $d(z)$ rather severely: neither the heights nor the positions of most peaks are predicted with even semi-quantitative accuracy. Still, the mean values of $Q_{zz}(z)$ are reasonably faithfully reproduced, as well as the fact that the density peaks are farther apart for homeotropic than for planar anchoring, as expected.

It is a nearly universal rule that the behaviour of $Q_{zz}(z)$ follows that of $d(z)$, i.e., regions of high density are also more highly ordered. The exceptions are the surface layers of homeotropically-anchored films, where there are very few but very strongly aligned particles (see figures 2 and 4).

In table 3 we present the approximate $L/\sigma_L = L^*/\kappa$ at which there is a crossover from homeotropic to planar 'bulk' alignment. Unsurprisingly, the agreement between theory and simulation is better for the larger elongation, $\kappa = 5$. Insight can be gained into the anchoring transition by noting that, in the limit of perfect orientational and positional order, the Helmholtz free energy of this system is minimized by the arrangement that maximizes the particle volume absorbed into the substrates. The homeotropic-to-planar transition is then given by equating the ratio of the volume absorbed into the substrates to the area occupied by the particle on the substrates (i.e., the projection of the particles onto the substrates) for the two key arrangements. In the limit of perfect order, symmetry details of the packing can be ignored in this calculation since they must be the same for both anchorings; the two arrangements will map onto each other via suitable affine transformations. These two competing tendencies yield a crossover needle length $L/\sigma_L = L^*/\kappa \sim 0.4817$ for $\kappa = 3$ and $L/\sigma_L = L^*/\kappa \sim 0.6084$ for $\kappa = 5$, which is in line with our results: in particular, it is an increasing function of κ. Such quantitative

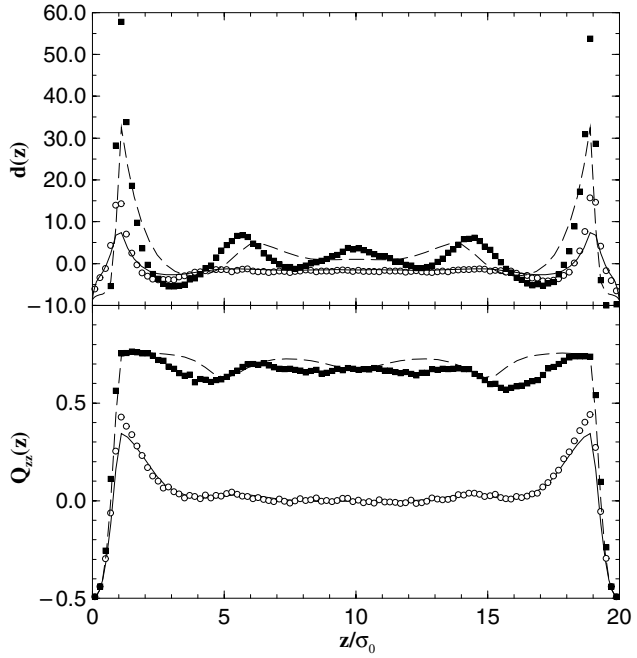

Figure 2. The same as figure 1, but for $L^* = 2.0$ ($L/\sigma_L = 0.4$). Now alignment at the higher density is homeotropic throughout most of the film, as can be seen from the fact that $Q_{zz}(z) > 0$ except in regions of width $\sim L/2 = 1.25\sigma_0$ close to the walls.

Table 3. Film alignment crosses over from homeotropic to planar for $L/\sigma_L = L^*/\kappa$ in each of the intervals shown. The data are from theory (th) and simulation (sim) (this work), and the analytical estimates of [11] (analyt).

κ	$(L/\sigma_L)^{\text{th}}$	$(L/\sigma_L)^{\text{sim}}$	$(L/\sigma_L)^{\text{analyt}}$
3	(0.55, 0.56)	(0.45, 0.46)	0.4817
5	(0.56, 0.58)	(0.50, 0.52)	0.6084

discrepancies as there are likely follow from having assumed (contrary to observation) that there is close packing at the walls: as we saw above, theory in particular systematically underestimates the contact densities; see [11] for details. As the bulk HGO fluid does not exhibit any smectic phases, we do not expect the crossover L to depend on system size, provided the latter is greater than twice the distance to which a single wall induces stratification.

Interestingly, on the homeotropic side just before (i.e., at L marginally below that of) the crossover, the density profiles exhibit very pronounced peaks and troughs, which smooth out dramatically once the system has gone planar; see figure 5. In particular, note the double-peaked structure close to the walls at the larger L, which suggests that the interface layers exhibit both planar and homeotropic features. As far as we can tell, the transition is fairly abrupt, occurring in an interval of L^* of width 0.1 (alternatively, in an interval of L/σ_L of width 0.02). Simulation results suggest [11] that there may be bistability close to the transition, i.e., both homeotropic and planar anchoring states are stable for the same L. We were able to get the theory to converge to the 'wrong' anchoring (homeotropic for $L^* = 2.9$, with higher free energy than planar) by strongly biassing the initial guess: more work is needed to establish whether this is real or an artefact of the numerical method.

Finally, attention is drawn to the fact that all comparisons in this section have been effected at constant density and varying L. This is the natural thing to do, as N, the particle number, and $|z_0^1 - z_0^2|$, the system size, are fixed in the MC simulations. Note, however, that because

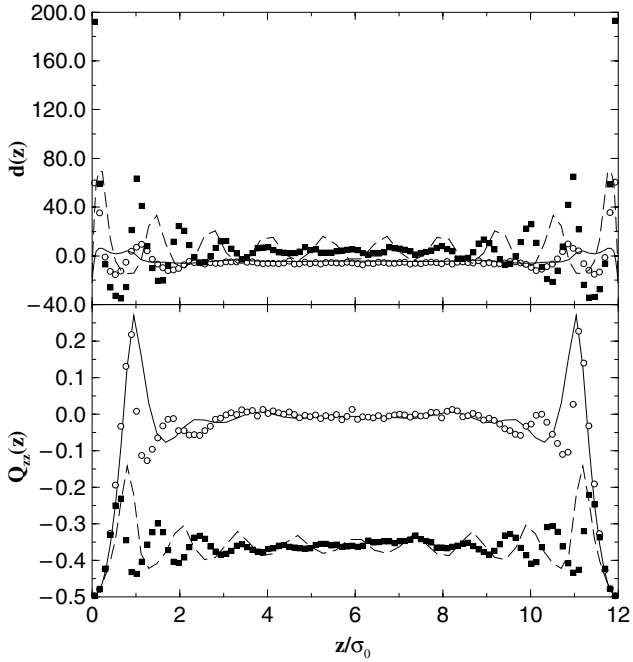

Figure 3. Scaled density $d(z)$ (top) and order parameter $Q_{zz}(z)$ (bottom) profiles for a symmetrical film of HGO particles of elongation $\kappa = 3$ and $L^* = 1.8$ ($L/\sigma_L = 0.6$), for $d_{\text{bulk}} = -3.392\,852\,98$ (solid curve and circles) and 7.321 422 42 (dashed curve and squares). Lines are from theory, symbols are from simulation. At the higher density, which lies in the nematic region of the bulk phase diagram, alignment is planar throughout the film, as in figure 1. Now the Onsager approximation severely underestimates the degree of structure of $d(z)$. See the text and table 2 for details.

particles can partially penetrate the substrates, the volume accessible to them is a function not just of $|z_0^1 - z_0^2|$, but also of L, the needle length: the smaller L, the deeper a particle can sink, and thus effectively the larger the system. It then follows that the *imposed* total density (which we referred to above as simply 'the density'), found by dividing the number of particles by the wall separation times the wall area, is not the *actual* or *true* density. It is possible to estimate the system volume increase as a function of the type of anchoring and ultimately of L, and thereby get the 'true' density [11]. Yet here we have elected not to do this and used instead the imposed, 'uncorrected' density: though it may not be an absolutely unambiguous descriptor in the microscopic sense, it is what is set in simulations and measured in experiments. Furthermore, in order to keep the 'true' density constant we would require knowledge of the actual system volume and therefore of what anchoring would come out of a given calculation or simulation prior to running it—a not impossible, but rather unwieldy, iterative task.

4. Conclusions

In this paper we have presented a density-functional treatment of an HGO fluid confined between parallel walls of tunable penetrability. Despite its simplicity, the Onsager approximation can in some cases yield semi-quantitative results for the density and orientational distribution of particles of elongation as small as $\kappa = 5$ (but not $\kappa = 3$). This simple model for the structure of the nematic matrix squeezed between tight-packed colloidal particles captures

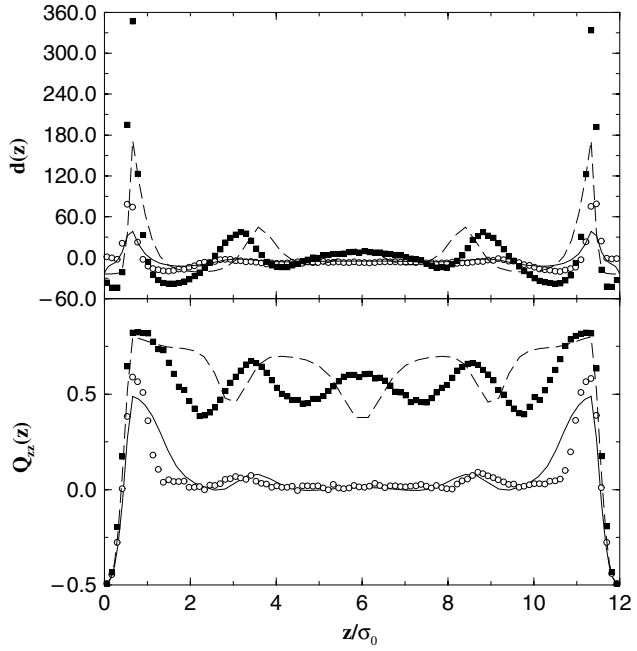

Figure 4. The same as figure 3, but for $L^* = 1.2$ ($L/\sigma_L = 0.4$). Now alignment at the higher density is homeotropic throughout most of the film but planar in regions of width $\sim L/2 = 0.6\sigma_0$ close to the walls, as in figure 2.

effects missed by the more current Frank and LdG theories, namely to do with layering. Moreover, the solution procedure also yields the free energy, thus making it possible to derive the effective interaction between walls/particles. This will be the subject of future work.

When comparing theory and simulation, account has to be taken of the fact that they yield rather different I–N transition densities and widths. This is due to our neglect of correlations of order higher than second-virial, which are relevant in the range of densities of interest. Greater predictive power would require a far more sophisticated approach, such as a weighted-density [25] or fundamental-measure [26] approximation. The development and implementation of such a scheme are, however, highly non-trivial. In keeping with our aim of assessing the validity and usefulness of the Onsager approach, we instead adapted a phenomenological scaling of the density first proposed by Allen and collaborators [24]. Agreement for symmetric films is fairly good, in spite of the smallness of κ, but its quality is strongly dependent on the accuracy of the isotropic and nematic coexistence densities as determined independently by either theory or simulation. We have not addressed the fact that these are (sometimes dramatically) shifted from their bulk values by both confinement and wall penetrability [11].

The theory can also be applied to hybrid films. It would be particularly interesting to see whether it is able to describe

(i) the more common uniform and bent-director structures already predicted [29] and observed [30];
(ii) the discontinuous transition between these two structures found by ourselves [10]; and
(iii) the more exotic biaxial structure in which two strata of film, each with a uniform director orientation dictated by the nearest wall, are separated by a sharp interface [31].

Both (ii) and (iii) depend crucially on the anchoring strengths at the two substrates being large and dissimilar or large and similar, respectively. However, preliminary calculations suggest that our chosen mechanism of making the walls partially penetrable to particles produces

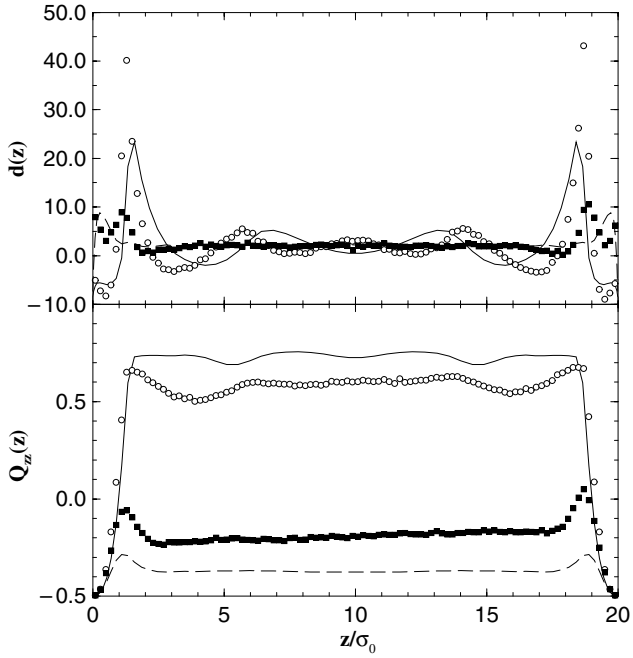

Figure 5. Scaled density $d(z)$ (top) and order parameter $Q_{zz}(z)$ (bottom) profiles for a symmetrical film of HGO particles of elongation $\kappa = 5$ and reduced density $d_{\text{bulk}} = 2.506\,024\,58$ on either side of the crossover from homeotropic to planar anchoring. Theory: $L^* = 2.8$ or $L/\sigma_L = 0.56$ (solid curve), $L^* = 2.9$ or $L/\sigma_L = 0.58$ (dashed curve). Simulation: $L^* = 2.5$ or $L/\sigma_L = 0.5$ (circles), $L^* = 2.6$ or $L/\sigma_L = 0.52$ (squares). Note the high degree of layering when the homeotropically aligned film is just about to go planar. See the text and table 3 for details.

much stronger homeotropic than parallel anchoring. This would need to be checked by a direct calculation of the anchoring energy, similar to that performed in [22]. A more ambitious aim would be to be able to shed some light on the observation by Vandenbrouck *et al* [32] of spinodal dewetting of the nematogen 5CB spun-cast onto silicon wafers, where hybrid anchoring was enforced by conflicting boundary conditions: orthogonal at the free surface, and planar at the silicon substrate. Such behaviour was initially interpreted in terms of a competition between elasticity and van der Waals forces [32], but subsequent arguments have related it to the fluctuation-induced interactions that underlie the pseudo-Casimir effect [33].

The present theory can be straightforwardly generalized to more sophisticated surface interactions, and also to mixtures of two or more types of hard body. One can envisage a very rich behaviour of a confined binary mixture where the two components have different easy axes at either substrate.

Acknowledgments

We are grateful to C M Care, A Chrzanowska, J R Henderson, Y Mao, A Poniewierski, E Velasco, P Ziherl and S Žumer for stimulating discussions. FB acknowledges Sheffield Hallam University's Materials Research Institute for a research student bursary.

References

[1] Stark H 2001 *Phys. Rep.* **351** 387
[2] Poulin P, Raghunathan V A, Richetti P and Roux D 1994 *J. Physique* II **4** 1557

Poulin P, Stark H, Lubensky T C and Weitz D A 1997 *Science* **275** 1770
[3] Zapotocky M, Ramos L, Poulin P, Lubensky T C and Weitz D A 1999 *Science* **283** 209
[4] Meeker S P, Poon W C K, Crain J and Terentjev E M 2000 *Phys. Rev.* E **61** R6083
Anderson V J, Terentjev E M, Meeker S P, Crain J and Poon W C K 2001 *Eur. Phys. J.* E **4** 11
Anderson V J and Terentjev E M 2001 *Eur. Phys. J.* E **4** 21
Petrov P G and Terentjev E M 2001 *Langmuir* **17** 2942
[5] Ruhwandl R W and Terentjev E M 1997 *Phys. Rev.* E **55** 2958
Ruhwandl R W and Terentjev E M 1997 *Phys. Rev.* E **56** 5561
Lubensky T C, Pettey D and Currier N 1998 *Phys. Rev.* E **57** 610
Poulin P and Weitz D A 1998 *Phys. Rev.* E **57** 626
Terentjev E M 1998 *Modern Aspects of Colloidal Dispersions* ed R H Ottewill and A R Rennie (Dordrecht: Kluwer) p 257
[6] Galatola P and Fournier J-B 1999 *Mol. Cryst. Liq. Cryst.* **330** 535
Borštnik A, Stark H and Žumer S 1999 *Phys. Rev.* E **60** 4210
Borštnik A, Stark H and Žumer S 2001 *Phys. Rev. Lett.* **86** 3915
Borštnik A, Stark H and Žumer S 2002 *Phys. Rev.* E **65** 032702
Galatola P, Fournier J-B and Stark H 2003 *Phys. Rev.* E **67** 031404
[7] Borštnik A, Stark H and Žumer S 2000 *Phys. Rev.* E **61** 2831
[8] Chrzanowska A, Teixeira P I C, Eherentraut H and Cleaver D J 2001 *J. Phys.: Condens. Matter* **13** 4715
[9] Groh B and Dietrich S 1999 *Phys. Rev.* E **59** 4216
Groh B 1999 *Phys. Rev.* E **59** 5606
[10] Cleaver D J and Teixeira P I C 2001 *Chem. Phys. Lett.* **338** 1
[11] Barmes F and Cleaver D J 2004 in preparation
[12] Padilla P and Velasco E 1997 *J. Chem. Phys.* **106** 10299
[13] de Miguel E and Martín del Rio E 2001 *J. Chem. Phys.* **115** 9072
[14] Perram J W and Wertheim M S 1985 *J. Comput. Phys.* **58** 409
Perram J W, Rasmussen J, Praestgaard E and Lebowitz J L 1996 *Phys. Rev.* E **54** 6565
[15] Allen M P, Evans G T, Frenkel D and Mulder B M 1993 *Adv. Chem. Phys.* **86** 1
[16] Bhethanabotla V R and Steele W 1987 *Mol. Phys.* **60** 249
[17] Rigby M 1989 *Mol. Phys.* **68** 687
Huang S L and Bhethanabotla V R 1999 *Int. J. Mod. Phys.* C **10** 361
[18] Evans R 1979 *Adv. Phys.* **28** 143
[19] Poniewierski A 1993 *Phys. Rev.* E **47** 3396
[20] Velasco E and Mederos L 1998 *J. Chem. Phys.* **109** 2361
[21] Chrzanowska A 2003 *J. Comput. Phys.* **191** 265
[22] Allen M P 1999 *Mol. Phys.* **96** 1391
Allen M P 2000 *J. Chem. Phys.* **112** 5447
[23] Telo da Gama M M 1984 *Mol. Phys.* **52** 585
Telo da Gama M M 1984 *Mol. Phys.* **52** 611
[24] McDonald A J, Allen M P and Schmid F 2001 *Phys. Rev.* E **63** 010701(R)
[25] Somoza A M and Tarazona P 1989 *J. Chem. Phys.* **91** 517
Velasco E, Mederos L and Sullivan D E 2000 *Phys. Rev.* E **62** 3708
[26] Cinacchi G and Schmid F 2002 *J. Phys.: Condens. Matter* **14** 12189
[27] Poniewierski A and Sluckin T J 1987 *Liq. Cryst.* **2** 281
[28] van Roij R, Dijkstra M and Evans R 2000 *Europhys. Lett.* **49** 350
van Roij R, Dijkstra M and Evans R 2000 *J. Chem. Phys.* **113** 7689
van Roij R, Dijkstra M and Evans R 2001 *Phys. Rev.* E **63** 051703
[29] Barbero G and Barberi R 1983 *J. Physique* **44** 609
[30] Blinov L M, Subachyus D B and Yablonsky S V 1991 *J. Physique* II **1** 459
Mazulla A, Ciuchi F and Sambles J R 2001 *Phys. Rev.* E **64** 021708
[31] Palffy-Muhoray P, Gartland E C and Kelly J R 1994 *Liq. Cryst.* **16** 713
Galabova H G, Kothekar N and Allender D W 1997 *Liq. Cryst.* **23** 803
Šarlah A and Žumer S 1999 *Phys. Rev.* E **60** 1821
Rodríguez-Ponce I, Romero-Enrique J M and Rull L F 2001 *Phys. Rev.* E **64** 051704
Chiccoli C, Pasini P, Šarlah A, Zannoni C and Žumer S 2003 *Phys. Rev.* E **67** 050703
[32] Vandenbrouck F, Valignat M P and Cazabat A M 1999 *Phys. Rev. Lett.* **82** 2693
[33] Ziherl P, Podgornik R and Žumer S 2000 *Phys. Rev. Lett.* **84** 1228
Ziherl P, Haddadan F K P, Podgornik R and Žumer S 2000 *Phys. Rev.* E **61** 5361